Journal of Physics: Condensed Matter

In situ NAP-XPS spectroscopy during methane dry reforming on ZrO_2/Pt(111) inverse model catalyst

To cite this article before publication: Christoph Rameshan *et al* 2018 *J. Phys.: Condens. Matter* in press https://doi.org/10.1088/1361-648X/aac6ff

In situ NAP-XPS Spectroscopy during Methane Dry Reforming on ZrO_2/Pt(111) Inverse Model Catalyst

C. Rameshan[1,], H. Li[1], K. Anic[1], M. Roiaz[1], V. Pramhaas[1], R. Rameshan[1,2], R. Blume[2], M. Hävecker[2], R. J. Knudsen[3], A. Knop-Gericke[2], G. Rupprechter[1,*]*

[1] *Institute of Materials Chemistry, Technische Universität Wien, Vienna, Austria*

[2] *Department of Inorganic Chemistry, Fritz Haber Institute of the Max Planck Society, Berlin, Germany*

[3] *Division of Synchrotron radiation research and the MAX IV Laboratory, Lund University, Lund, Sweden*

Corresponding Authors:
christoph.rameshan@tuwien.ac.at
guenther.rupprechter@tuwien.ac.at

Abstract

Due to the need of sustainable energy sources, methane dry reforming (MDR) is a useful reaction for the conversion of the greenhouse gases CH_4 and CO_2 to synthesis gas ($CO + H_2$). Syngas is the basis for a wide range of commodity chemicals and can be utilized for fuel production via Fischer–Tropsch (FT) synthesis. The current study focuses on spectroscopic investigations of the surface and reaction properties of a ZrO_2/Pt inverse model catalyst, i.e. ZrO_2 particles (islands) grown on a Pt(111) single crystal, with emphasis on *in situ* near ambient pressure X-ray photoelectron spectroscopy (NAP-XPS) during MDR reaction. In comparison to technological systems, model catalysts facilitate characterization of the surface (oxidation) state, surface adsorbates, and the role of the metal-support interface. Using XPS and infrared reflection absorption spectroscopy (IRAS) we demonstrate that under reducing conditions (UHV or CH_4) the ZrO_2 particles transformed to an ultrathin ZrO_2 film that started to cover (wet) the Pt surface, paralleled by a decrease in surface/interface oxygen. In contrast, (more oxidizing) dry reforming conditions with a 1:1 ratio of CH_4 and CO_2 were stabilizing the ZrO_2 particles on the model catalyst surface, as revealed by *in situ* XPS. Carbon deposits resulting from CH_4 dissociation were easily removed by CO_2 or by switching to dry reforming

conditions (673 – 873 K). Thus, at these temperatures the active Pt surface remained free of carbon deposits, also preserving the ZrO_2/Pt interface.

Key Words: inverse model catalyst, *in situ* XPS, IRAS, TPD, methane dry reforming, surface structure, catalysis

1. Introduction

Fossil fuels still represent the major energy source of the globalized economy and the annually growing consumption creates great environmental challenges due to increasing levels of greenhouse gases [1, 2]. Methane and carbon dioxide constitute a major part of greenhouse emissions with strong impact on global warming [3]. Since fossil fuels are limited there are great efforts in finding new, renewable and sustainable energy sources [4]. The conversion of small carbon containing molecules such as CH_4 to syngas (mixture of CO and H_2) may be part of possible solutions. Syngas is a building block for valuable liquid fuels and chemicals such as longer chain hydrocarbons produced by the Fischer-Tropsch (FT) process, or for synthesis of methanol and dimethylether [5-7].

The industrially relevant processes for syngas production include methane steam reforming, partial oxidation of methane with oxygen or air, and methane dry reforming (MDR) with carbon dioxide [3, 8]. Methane steam reforming produces a H_2/CO ratio of 3 [9] that is higher than that required for Fischer-Tropsch or methanol synthesis (H_2/CO = 2) [10]. Partial methane oxidation (H_2/CO = 2) is favourable for production of heavier hydrocarbons and naphtha [11] and has high conversion rates and high selectivity [12], but the exothermic nature of the reaction has drawbacks (e.g. heat removal) [8].

Dry reforming of methane ($CH_4 + CO_2 \rightarrow 2\ CO + 2\ H_2$) has several environmental benefits: it can utilize biogas as source [13, 14] (biogas from anaerobic decomposition of organic material produces nearly equal CH_4 and CO_2 concentrations [15]) and, more important, it reduces emissions of greenhouse gases CH_4 and CO_2 by transforming them into value-added syngas [16]. Natural gas with a high CO_2 content can also be transformed into fuel via MDR [5]. The lower syngas ratio (H_2/CO = 1) of MDR is suitable for the synthesis of oxygenated chemicals [17] and hydrocarbons from FT synthesis. Methane dry reforming has also been considered as a suitable route to thermochemically convert solar energy to fuel [18, 19]. Ross et al. reported that MDR has 20% lower operating costs than the other CH_4 reforming processes [20]. Therefore, we have focused on MDR in the current study.

The most widely used metal for dry MDR is Ni [21-25], but Ni-based catalysts often undergo severe deactivation (loss of activity) with time due to carbon deposition (carbon nanotube formation) [3, 26, 27]. When using noble metal catalysts the coking problem can be avoided or reduced. Therefore, MDR has been studied over a series of supported Pt, Pd, Rh, and Ru catalysts [1, 28-34] but also Co and Fe have been investigated [3, 16]. In terms of performance, M. Németh et al. demonstrated comparable catalytic activity of Ni-ZrO_2 and Pt-ZrO_2 powder catalysts (1 wt% metal) [35]. However, an apparent drawback of noble metal systems is their high cost. A possible solution is the addition of small amounts of noble metals (Rh, Ru, Pd, and Pt) to Ni catalysts, which leads to improved catalytic properties and lower sensitivity to carbon deposition, maintaining a lower materials cost [3, 36]. Furthermore, the use of bimetallic nanoparticles may also improve the catalytic performance [1, 3, 37-39].

As controversially discussed in the literature, the mechanism of methane dry reforming seems bi-functional. CH_4 is activated on the metal via dissociation [40], whereas CO_2 is activated on acidic/basic supports. On acidic supports, CO_2 is activated via formation of formates (reaction with the surface hydroxyls) and on basic supports by forming oxy-carbonates [41, 42]. For catalysts with relatively inert supports like SiO_2 the mechanism is considered to follow a mono-functional pathway, with only the metal activating both reactants [1, 3]. Apart from the different possible reaction pathways, the role of the metal-oxide interface has been vividly discussed [41, 43, 44].

Clearly, microscopic mechanisms of the interplay of metal and support, including potential structure changes under reaction conditions (e.g. strong metal support interaction, SMSI, and the resulting loss of activity) [45, 46], need to be better understood, e.g. by utilizing a surface science approach.

Based on this motivation we have carried out a systematic surface-sensitive study of the interaction of CH_4/CO_2 with an inverse model catalyst, i.e. ZrO_2 particles/islands supported on a Pt(111) single crystal (also using Pt(111) as a support-free reference). Inverse model catalyst surfaces allow – when compared to powder systems - better spectroscopic identification of the surface state, metal-support interactions and of the role of the interface [47]. Accordingly, the ZrO_2/Pt(111) model catalyst was characterized by temperature programmed desorption (TPD), infrared spectroscopy (IRAS), and X-ray photoelectron spectroscopy (XPS) (the latter also applied *in situ* during catalytic reaction).

2. Experimental

Laboratory Measurements

The laboratory measurements (TPD and IRAS) were performed in a custom-built UHV chamber that was described elsewhere [48-50]. The preparation chamber is equipped with a differentially-pumped quadrupole mass spectrometer (MKS eVison+), LEED optics (SPECS ERLEED 1000-A), and a standard X-ray source (SPECS XR 50, with AlKα and MgKα anode) combined with a SPECS EA 150 PHOIBOS hemispherical analyzer. The UHV-compatible high pressure cell ("Rupprechter design") [50, 51] is connected to a Fourier transform IR spectrometer (Bruker Vertex 60v) and a ZnSe photoelastic modulator operating at 34 kHz.

The Pt(111) single crystal (MaTek) was cleaned by sputtering with 1 kV Ar^+ ions (p Ar = 5 × 10^{-6} mbar, sputtering current = 2 μA) for 45 min followed by thermal annealing to 1070 K. Crystal cleanliness was confirmed by XPS. For the inverse model system, ZrO_2 particles were prepared on the Pt(111) single crystal by sputter deposition of Zr (from a foil, Alfa Aeser, purity 99.5%) in 5 × 10^{-6} mbar O_2 at RT, utilizing a custom-built sputter source for precise and reproducible deposition amounts [52]. The nominal thickness of the as-deposited ZrO_2 film was 0.3 nm (the thickness of a (111) oriented bulk ZrO_2 (O-Zr-O) layer is 0.295 nm [53]). Sputter deposition by this special technique leads to the growth of uniformly distributed ZrO_2 islands, as observed by scanning tunneling microscopy (STM) [54]. Directly after deposition, the sample was annealed in 5 × 10^{-7} mbar O_2 to 873 K to fully oxidize the deposited ZrO_x to ZrO_2 leading to the formation of larger ZrO_2 islands on Pt(111). As shown in the following section, the coverage of the ZrO_2 islands on Pt(111) was about half of a monolayer. Based on the nominally deposited 0.3 nm (monolayer), this would result in ZrO_2 islands with an average thickness of two oxide layers (double layer O-Zr-O-Zr-O). All experiments (lab and synchrotron) were performed on the same sample.

Only high purity gases from Messer Austria were used for all experiments. The purity of oxygen and hydrogen was 5.0, CO_2 was 4.8, CH_4 was 4.5 and the purity of CO was 4.7. Additionally, in order to avoid carbonyl contaminations, a carbonyl absorber cartridge was installed in the CO gasline [49].

Experiments in the low pressure range were performed both in the UHV preparation chamber and high pressure cell. Dosing of gases was carried out using a high precision leak valve. The Langmuir coverage was calculated assuming a sticking coefficient of unity. The IRAS measurements of CO adsorption were carried out under UHV in the high pressure cell

(spectral range 1500 to 2600 cm^{-1}). Data processing was performed according to procedures described by P. Hollins [55].

TPD spectra were collected by a differentially-pumped MKS eVision+ quadrupole mass spectrometer, and temperature ramping was performed by a Eurotherm 3216 PID controller, with a heating rate of 60 K/min [53].

The ability to regenerate ZrO_2 particles after exposure to air was confirmed prior to the synchrotron measurements. This was important as the sample was prepared in the Vienna lab and then transported to the respective synchrotron facility. For this, the sample was removed from the UHV chamber and exposed to air for 24 – 48 h. Afterwards, the same sample was again mounted to the manipulator of the UHV chamber. After a reoxidation cycle, the original chemical composition and surface structure of the ZrO_2 islands was re-established, as confirmed by XPS and TPD.

Synchrotron Measurements

The methane dry reforming *in situ* experiments were conducted at two different synchrotron facilities due to different experimental requirements. The ISISS end station at HZB/BESSY is capable to run *in situ* experiments up to 1000 K, which is required for the methane dry reforming catalytic measurements. However, the system is not optimized for true UHV studies (i.e. the base pressure of the *in situ* cell is only in the mid 10^{-8} mbar range). In comparison, the SPECIES end station at the MAX IV laboratory is limited to a maximum reaction temperature of 673 K, which is below real dry reforming operational temperatures. However, the special design of this system allows true UHV investigations and (clean) *in situ* experiments. This is important for the characterisation of the as-prepared state of the model catalyst and the initial exposure to the reactive gas environment. Nevertheless, benchmark experiments ensured that the experimental results of both beamlines were compatible.

Bessy Setup

In situ experiments were performed at the ISISS beam line of the HZB/BESSY II synchrotron in Berlin with a near-ambient pressure high energy X-ray photoelectron spectroscopy (NAP-HE-XPS) setup, which enables measurements at elevated pressures (up to 7 mbar) with photon energies ranging from ~80 up to 2000 eV. The main parts are a “high pressure” chamber with an attached differentially-pumped hemispherical analyser (modified SPECS Phoibos 150) including a 2D delay line detector. A detailed description of the near-ambient pressure XPS-setup is given in ref. [56]. Samples were heated via a tantalum back sheet using

an infrared laser. The temperature was monitored with a pyrometer measuring the surface temperature, as well as by a thermocouple.

MAX IV Lab Setup

In situ near ambient pressure X-ray photoelectron spectroscopy (NAP-XPS) was performed at the high resolution X-ray photoemission spectroscopy XPS endstation SPECIES at the MAX IV Laboratory. The setup and beamline is described in detail in ref. [57, 58]. Again, photon energies from ~80 to 2000 eV could be chosen. The system was capable of performing ambient pressure and true UHV experiments. This is realized by using a retractable 'high-pressure cell', which can be docked to the front aperture of the SPECS PHOIBOS 150 NAP analyser for ambient pressure experiments. During *in situ* measurements only the cell was filled with gases, while the analysis chamber remained evacuated. Heating was achieved through electron bombardment of the vacuum side of the wall behind the sample seat of the high-pressure cell. With this design no hot filament was exposed to the gas environment. The sample temperature was measured with a chromel-alumel thermocouple wire pair mounted on the transferable sample holder.

Both *in situ* setups are designed as continuous catalytic flow cells with gas analysis by mass spectrometry. For catalytic reactions, the interaction of the model catalysts surface with pure CH_4 or CO_2 was studied first (0.1 mbar in both cases). For the MDR reaction a total pressure of 0.2 mbar with 1:1 composition of CH_4 and CO_2 was used (during the single bunch beamtime higher pressures were not accessible). During reaction the temperature was varied stepwise from RT to 873 K. Reaction educts and products were followed by mass spectrometry. Additionally, a clean Pt(111) single crystal was used as reference for the MDR reaction and for peak assignments.

Surface sensitive *in situ* XPS spectra were obtained with different incident photon energies (140 eV for VB, 210 eV for Pt 4f, 320 eV for Zr 3d, 420 eV for C 1s, and 670 eV for O 1s). These correspond to kinetic photoelectron energies between 130 and 150 eV, which leads to almost equal information depth (inelastic mean free path, IMFP) of 0.5−0.6 nm, according to NIST Standard Reference Database [59]. In case of depth profiling measurements, the photon energies were increased in multiple steps, resulting in photoelectron energies up to 740 eV, and an information depth (IMFP) up to 1.5 nm. After each change of excitation energy a spectrum of the Fermi edge was recorded for calibration of the binding energy axis. All

spectra were referenced to the Fermi edge, which is necessary due to monochromator mechanics at the synchrotron [60].

The spectra were fitted with CasaXPS, using a Shirley background subtraction and mixed Gaussian−Lorentzian (GL) peak shapes for the Zr, C, and O components. The Zr 3d region was fitted with doublets, restricted by equal FWHM, fixed doublet separation of 2.4 eV (spin orbit splitting) and an area ratio of 2:3 [53]. The assignment of the signals to Zr-clusters and Zr-film was based on previous studies by Li et al. [53]. For the Pt 4f signal an asymmetry function was used for peak fitting. The parameters for the asymmetry were obtained from measuring the clean Pt(111) reference sample. The Pt 4f signal was fitted with doublets with a fixed separation of 3.3 eV and an area ratio of 3:4.

Possible beam damage or beam-induced surface modifications were examined prior to the actual *in situ* experiments. This was achieved by measuring different positions (spots) on the sample surface (in equilibrium gas pressure) upon using different beam exposure times [60]. Based on the comparison of the results, which indicated no differences for different exposure times, X-ray beam damage could be excluded.

Additional *in situ* measurements were carried out on a Pt(111) single crystal, for comparison with the inverse model system and for providing reference data for fitting.

3. Results

3.1. Structural characterisation by XPS, IR and TPD

Prior to the actual methane dry reforming experiments, a detailed characterisation of the as-prepared (oxidized) and annealed ZrO_2/Pt(111) inverse model catalyst surface was carried out to determine structure and thermal stability in UHV. Accordingly, the ZrO_2/Pt(111) system was heated stepwise to 673 K in UHV while measuring surface-sensitive XPS spectra at MAX IV (figure 1).

In 4.5 x 10^{-5} mbar O_2 at 573 K a distinct Zr3d feature could be observed at 181.7 eV (figure 1a), which agrees with values reported for supported ZrO_2 with cluster-like structure [53, 61]. The Zr 3d signal was slightly shifted to lower binding energies (BE), presumably due to the presence of adsorbed oxygen, see the detailed discussion below (section 3.2 in-situ XPS). Upon pumping off the O_2 background and heating the model catalyst to 473 K in UHV, the main ZrO_2 signal shifted to 182.4 eV (expected for ZrO_2 islands), and an additional

component appeared at 181.1 eV (figure 1). The peak shift of the main signal was likely caused by desorption of adsorbed oxygen. In line with our previous studies on supported thin ZrO_2 films the species at 181.1 eV can be attributed to the growth of an ultrathin ZrO_2 film on the Pt(111) surface (i.e only one tri-layer of ZrO_2) [53] (see also the model in the discussion section). The 0.4 eV lower BE of the tri-layer in our previous study can be explained by the different substrate materials (Pt vs. Pt_3Zr) and the different morphology (islands vs. continuous film). The driving force of film growth is that at elevated temperatures and in UHV the ultrathin ZrO_2 film is thermodynamically more stable than thicker ZrO_2 nanoparticles or clusters [53, 62] (up to the point when the oxide decomposes, >1173 K [63]). When the temperature was raised to 573 and 673 K in UHV (figures 1), the ZrO_2 trilayer film signal further increased (i.e. up to ~20% of the Zr 3d signal at 673 K), while the intensity of the cluster-related signal decreased. The formation of a PtZr alloy during annealing could not be observed, as the expected signal at 179.6 eV was absent (see figure 1) [53]. Also, the Pt4f signal did not change during UHV annealing to 673 K (see supporting information figure S1). Upon reoxidation in O_2 atmosphere ($p = 4.5 \times 10^{-5}$ mbar, 573 K, 10 min), the initial state of the surface with only ZrO_2 islands (on average a double-layer) was regenerated, i.e. the observed spreading of ZrO_2 on Pt(111) was reversible.

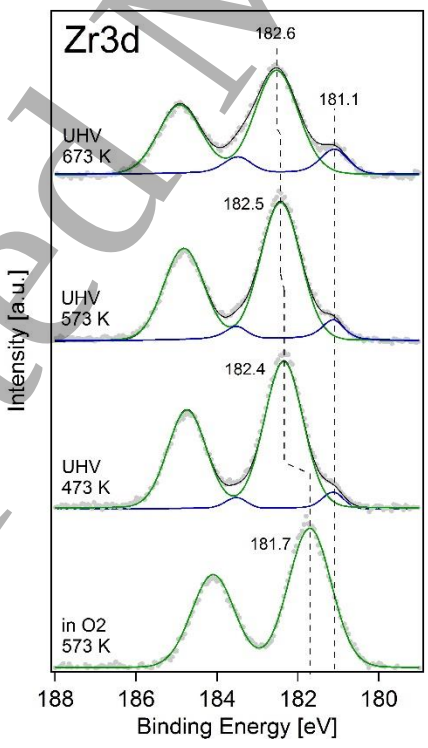

Figure 1: Zr 3d spectra of the as-deposited and oxidized ZrO_2 nanoparticles ($p(O_2)$ = 4.5 x 10^{-5} mbar) and after stepwise annealing to 673 K in UHV. With increasing temperature, the evolution of an increasing Zr film signal at 181.1 eV was observed.

To learn more about the structure of the ZrO_2/Pt(111) inverse model catalyst, infrared measurements were performed, using CO as probe molecule (figure 2a). After exposure of the (oxidized) inverse model catalyst surface to 4 L CO at RT, a distinct feature at 2090 cm^{-1} was observed, characteristic of on-top CO adsorbed on the uncovered Pt(111) surface [64] (CO does not adsorb on the ZrO_2 surface at these conditions [53]). To quantify the amount of adsorbed CO, TPD spectra were acquired, again after 4 L CO were dosed to the sample surface at 300 K (figure 2b). A desorption feature with a peak maximum at ~390 K originating from Pt(111) was observed [65] (corresponding to a desorption energy of ~98 kJ/mol). By comparison with the area of desorption from a clean Pt(111) surface (with a CO saturation coverage of 0.5 ML at 300 K), it can be estimated that ~50% of the Pt surface was covered by the ZrO_2 nanoparticles/islands. Accordingly, these islands must be ~0.6 nm in thickness but their average size is currently unknown (note that Lackner et al. reported the growth of small islands (about 2-5 nm in size) when depositing ZrO_2 by the same method on a Rh(111) single crystal [54]).

Upon annealing ZrO_2/Pt(111) in UHV to 423 K (figure 2a) and re-dosing 4 L CO at RT, the amount of adsorbed CO was reduced and shifted to lower wavenumber (~2080 cm^{-1}). This is in line with XPS spectra (figure 1), indicating the onset of formation of an ultrathin ZrO_2 layer wetting the Pt(111) surface and therefore blocking adsorption sites. The redshift may be due to lower CO coverage and/or lower CO ordering (that would cause reduced dipole-dipole-interaction) [65-67]. A roughening of the Pt surface (that would also cause a red-shift of CO) is also possible [68].

When the surface was heated to even higher temperatures (523, 623 and 723 K) the CO signal intensity decreased further, until it was nearly undistinguishable from the background noise. At the highest temperature, the signal shifted down to 2070 cm^{-1}. Again, this is in line with the increasing signal of the spreading ultrathin ZrO_2 film covering more and more of the Pt(111) surface. After this series of IR spectra, the model catalyst surface was reoxidised and again exposed to 4 L CO at RT (figure 2a, top spectrum). The obtained infrared signal was comparable to the initial signal after model catalyst preparation, with a peak at 2090 cm^{-1} of similar signal intensity. The XPS and infrared data point to the conclusion that upon UHV annealing (reduction) the ZrO_2 islands started to wet the Pt surface whereas exposure of the

inverse model catalyst to oxidising conditions re-established the ZrO_2 islands/clusters and the initial amount of uncovered Pt(111). This is an important finding, because it is important to know whether under dry reforming reaction conditions the ZrO_2 islands may wet/cover the Pt(111) surface, causing a pronounced surface modification of the catalyst (that may be beneficial or detremential for the catalytic performance).

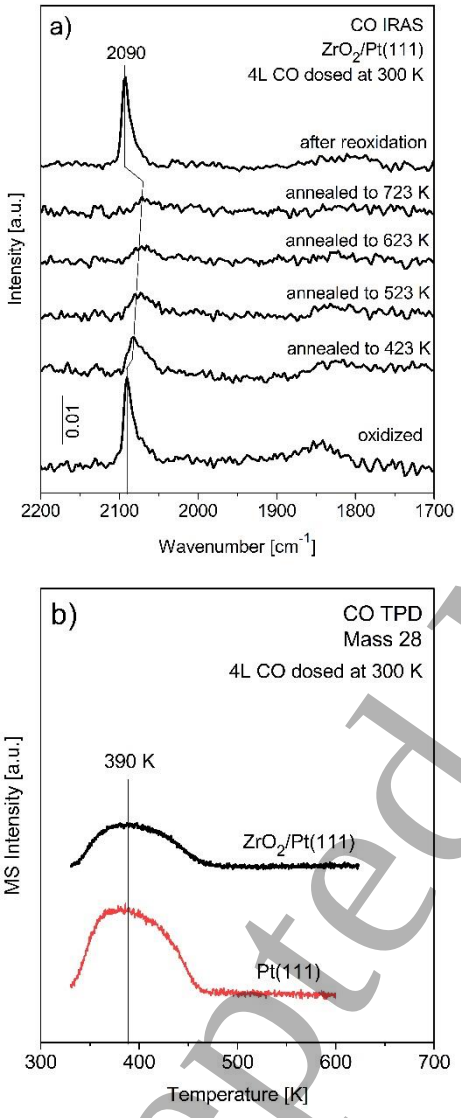

Figure 2: a) Infrared spectra after exposure of 4L CO to the as-prepared (oxidized) and UHV-annealed ZrO_2 nanoparticles on Pt(111). The signal of on-top CO is decreasing with increasing annealing temperature. The initial spectrum with a signal at 2090 cm^{-1} can be retrieved after reoxidation of the inverse model catalyst surface. b) CO TPD spectra upon exposure to 4 L CO at 300 K. The bottom spectrum (red) shows desorption from a clean

Pt(111) surface (0.5 ML coverage) as reference. The top TPD spectrum (black) was collected from the as-prepared and oxidized ZrO_2/Pt(111) sample.

3.2 *In situ* NAP XPS Studies

Before the actual methane dry reforming experiments, the interaction of the inverse model catalyst surface with the individual reactants (i.e. with CH_4 or CO_2 separately) was tested. This provides useful information on the reactivity of the respective molecule on the surface and its temperature-dependent effect on the surface structure/composition.

CH_4 exposure to ZrO_2/Pt(111)

Figure 3 summarizes the *in situ* XPS results for exposure to 0.1 mbar CH_4 at increasing temperature (measured at BESSY).

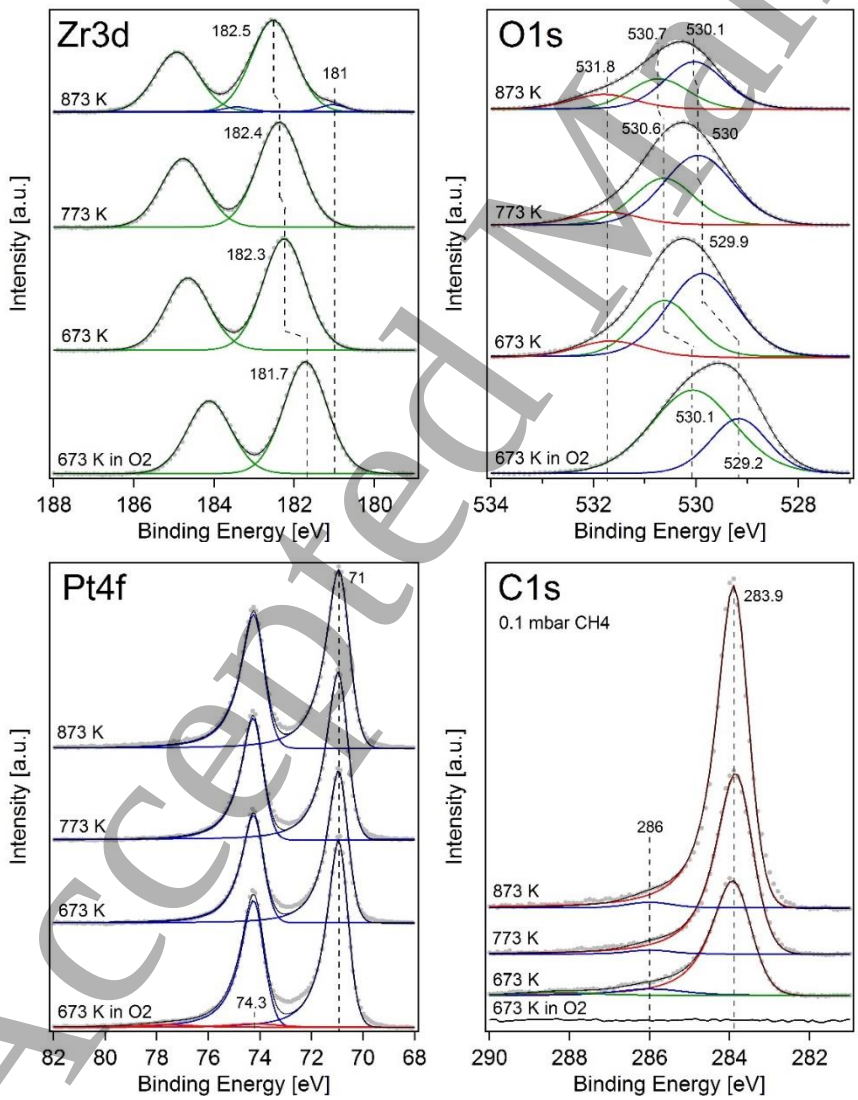

Figure 3: In situ XPS spectra of the ZrO_2/Pt(111) inverse model catalyst during 0.1 mbar CH_4 exposure at increasing reaction temperature. The bottom spectra were recorded prior to CH_4 exposure in $p(O_2) = 4.5 \times 10^{-5}$ mbar at 673 K.

For the pristine model catalyst surface (regenerated at 673 K in 4.5 x 10^{-5} mbar O_2) the binding energies are 181.7 eV for Zr 3d, corresponding to the ZrO_2 particles/islands, and 71 eV for Pt 4f of the Pt(111) substrate (metallic Pt) [69]. No carbon traces were observed on the surface. Upon dosing of 0.1 mbar CH_4 at 673 K the signal of the ZrO_2 clusters shifted to 182.3 eV. A similar shift of 0.6 eV was observed in the O 1s signal, whereas the Pt 4f signal stayed at 71 eV.

To explain the binding energy shift of the Zr 3d and O 1s signals a closer look on the O 1s peak components is needed (note that the peak fitting for O 1s is strongly simplified as multiple factors have to be considered, see the supporting information for a detailed discussion). Upon oxidative treatment two components could be observed: a low BE component at ~529.2 eV (blue, figure 3) whose intensity turned out to be rather unaffected by the atmosphere (pointing to a "island-bulk like" ZrO_2), and a high BE component at ~530.1 eV (green), whose intensity depended on the atmosphere (pointing to surface or interface oxygen species that can be removed or replenished; e.g. O from ZrO_2 at the interface with possible charge transfer from O to Pt support [70, 71]). Upon switching from O_2 to CH_4 atmosphere, which produces C and H on the free Pt surface, the surface/interface oxygen vanished, leading to a decrease in intensity of the high BE (530.7 eV, green) component.

Note that at the same time the entire O 1s and Zr 3d signals shifted to higher BE. With increasing temperature, the Zr 3d signal shifted even more whereas O1s did not. When comparing the O 1s spectra of the experiments described below (pure CO_2, switching from CH_4 to CO_2 and dry reforming with CO_2/CH_4) a clear trend can be identified. For oxygen-rich/oxidizing conditions an increased intensity of the high BE component (green) can be found and additionally a total shift of Zr 3d and O1s to lower BE is observed. In contrast, for reducing conditions (UHV or CH_4) the intensity of the high BE component of O1s was much lower and peaks of O, Zr were located at higher BE. For the initial state of the (oxidized) model catalyst surface or for more oxidizing reaction conditions, we can thus propose that the higher abundance of surface/interface oxygen lead to a relative downshift of the O1s and Zr3d signals. For reducing conditions (UHV, CH_4), less surface/interface oxygen is present and thus the Zr 3d and O1s signals are located at the expected values. Following this discussion,

Norton et al. reported that the surface work function depends on the coverage of adsorbate molecules, as shown for CO adsorption on Pt(111) [72].

In the C 1s spectra the formation of graphitic carbon (283.9 eV) was observed at 673 K. Also, trace amounts of carbonylic/carboxylic species (286 eV) were present with a corresponding component in the O 1s spectra at 531.8 eV. These carbon species result from the dehydrogenation of CH_4 on Pt [73] and reaction of C/CH_x species with surface oxygen. Similarly, Fuhrmann et al. showed that upon CH_4 adsorption and dehydrogenation on Pt(111) above 550 K the dominant species formed was graphitic carbon [74]. For the oxidized surface (673 K, $p(O_2) = 4.5 \times 10^{-5}$ mbar) trace amounts of PtO_x (74.3 eV) were also observed in the Pt4f spectra, which vanished upon CH_4 exposure.

Upon raising the temperature to 773 K, the amount of graphitic carbon on the surface increased, as more CH_4 was dehydrogenated to carbon. In the Zr 3d signal, a small shift to 182.4 eV was observed, whereas the Pt 4f and O 1s spectra did not change significantly. At the highest temperature (873 K) the amount of surface carbon drastically increased. Also, the Zr 3d signal showed some major changes. Again, the signal of the ZrO_2 clusters shifted further to higher BE (182.5 eV), and the evolution of a new small signal at 181 eV was observed. As already described in the previous section, this results from the formation of small patches of a ZrO_2 trilayer film on the surface [53]. Again, the Pt 4f signal did not change, excluding the formation of a PtZr alloy or other changes of the substrate material (see supporting information for further discussion on the limits of spectral resolution for Pt 4f). When switching back to oxidative conditions (673 K in 4.5×10^{-5} mbar O_2), as before CH_4 exposure, the signals of Zr 3d and O 1s shifted back to their initial state and all carbon was removed from the surface.

CO_2 exposure to ZrO_2/Pt(111)

In the next step, the interaction of CO_2 with the ZrO_2/Pt(111) model catalyst surface was studied by introducing 0.1 mbar CO_2 into the *in situ* cell at 673 K, increasing the temperature stepwise to 873 K while measuring *in situ* XPS spectra. Similar to the CH_4 experiment, the position of the Zr 3d signal before CO_2 exposure was at 181.8 eV. In contrast, the CO_2 atmosphere caused no significant change of the Zr 3d peak position and composition for all temperatures (673, 773 and 873 K, see supporting information figure S2). Compared to exposure to pure CH_4, the formation of a ZrO_2 trilayer film at 873 K was not observed, indicating that CO_2 stabilized the cluster structure (i.e. the gas atmosphere has a rather

oxidizing potential which maintains the particle structure). Additionally, no significant changes were observed for C 1s, O 1s and Pt 4f. No carbon formation occurred at all temperatures and the Pt 4f signal was constant at 71 eV. The peak maxima of O1s stayed between 529.6 and 529.8 eV without major changes of the peak shape. This leads to the conclusion that CO_2 did not alter the model catalyst surface (and did not remove surface/interface oxygen) but it seems to have a stabilizing effect on the ZrO_2 particles (see also the model in figure 6). As shown in the previous section (figure 1), in UHV the formation of the ZrO_2 ultrathin film was observed already at 473 K.

$CH_4 + CO_2$ switching on ZrO_2/Pt(111)

Following the studies of the interaction with the individual reactants, we have examined the effect of switching from 0.1 mbar CH_4 (mainly leading to carbon formation on the surface) to 0.1 mbar of CO_2. As shown in figure 4, the entire C1s signal immediately vanished after switching from CH_4 to CO_2 atmosphere at 673 K.

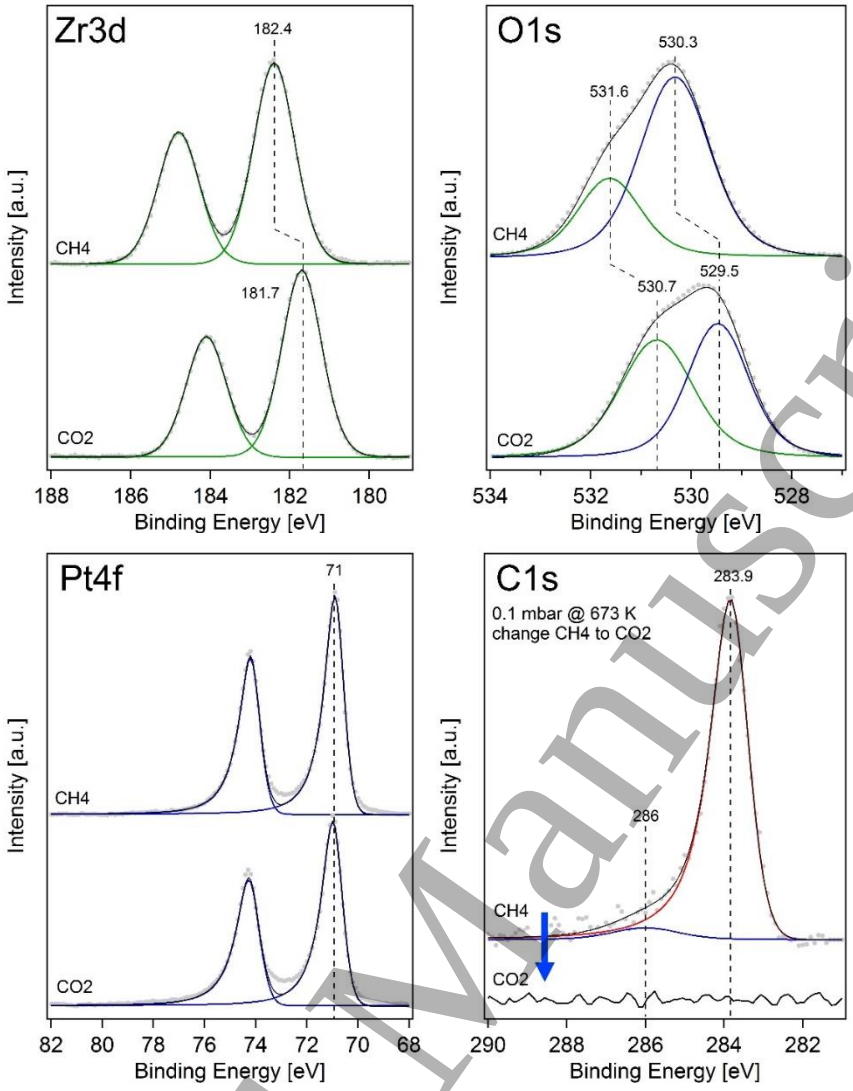

Figure 4: In situ XPS spectra of the ZrO_2/Pt(111) inverse model catalyst while switching from 0.1 mbar CH_4 to 0.1 mbar CO_2 at 673 K. A complete removal of the carbon species was observed.

The pathway for surface carbon removal under these conditions is via the Boudouard-reaction ($C + CO_2 \rightarrow 2\ CO$) with CO_2 reacting with the surface carbon [75]. For MDR on noble metal catalysts, Qin et al. also reported the efficient removal of surface carbon via this pathway for Rh, Ru, Ir, Pd and Pt supported on MgO [76].

When changing from (reducing) CH_4 to CO_2 the Zr 3d signal shifted from 182.4 to 181.7 eV and the O 1s spectra shifted from 530.3 (531.6) to 529.5 (530.7) eV. Apparently, CO_2 has an oxidizing effect ($CO_2 \rightarrow CO + O$), most likely via CO_2 activation at the ZrO_2/Pt interface and/or the (reduced) ZrO_2 islands. This leads to re-oxidation of the reduced surface/interface sites, as deduced from the strong intensity increase of the O1s component at higher BE (green) upon changing from reducing (CH_4) to more oxidizing conditions (CO_2). This is

attributed to the changing gas phase and the resulting surface work function change of the ZrO_2 particles, as discussed above. The Pt 4f signal was not affected with a constant peak position at 71 eV.

Reference measurements on pure Pt(111) (see supporting information S3) showed that the removal of surface carbon by CO_2 also occurs in the absence of the ZrO_2 particles/islands, indicating that Pt is catalysing the carbon removal by CO_2. Unfortunately, the amount of surface carbon was too low to obtain meaningful catalytic data (by CO mass spectrometer detection) to clarify whether the ZrO_2 support has an additional promoting effect on CO_2 activation and on carbon removal.

$CH_4 + CO_2$ mixture on ZrO_2/Pt(111)

After static and switching studies of the individual reactants, the actual methane dry reforming reaction was examined *in situ*. Following the usual oxidative treatment of the ZrO_2/Pt(111) inverse model catalyst (673 K, $p(O_2) = 4.7 \times 10^{-5}$ mbar), a total pressure of 0.2 mbar of CH_4 and CO_2 (1:1 ratio) was introduced into the HP cell at 673 K (figure 5).

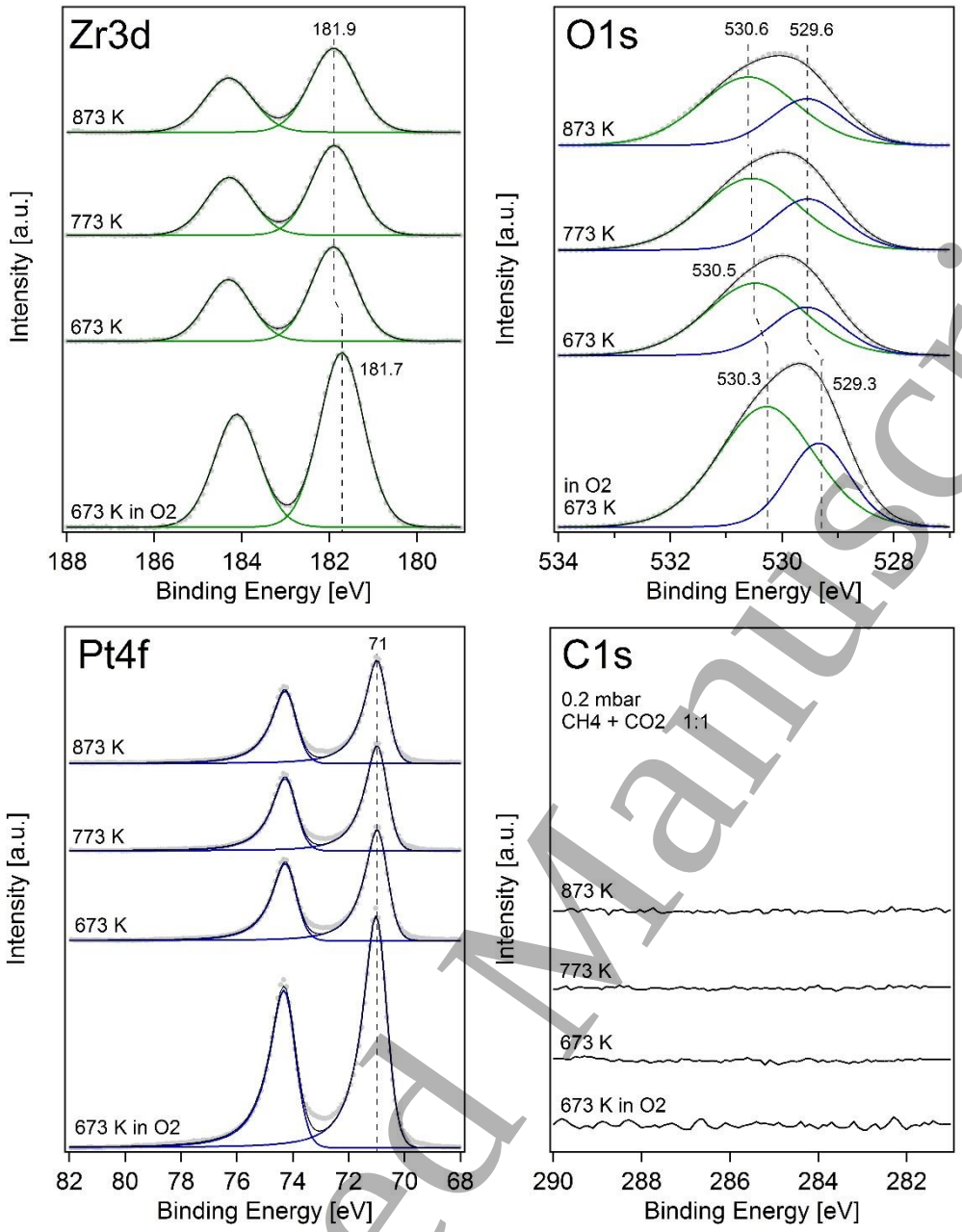

Figure 5: In situ XPS spectra of the ZrO_2/Pt(111) inverse model catalyst during methane dry reforming reaction (flow of 0.1 mbar CH_4 + 0.1 mbar CO_2) at increasing reaction temperature. The bottom spectra were recorded in oxygen environment (673 K, $p(O_2) = 4.7 \times 10^{-5}$ mbar), prior to exposure to the reaction mixture.

Upon exposing the surface to the reactive gas atmosphere, the Zr 3d signal shifted from 181.7 to 181.9 eV. A similar small shift was observed in the O 1s spectra (529.3/530.3 to 529.6/530.6 eV). As discussed earlier, the reason for the peak shifts of Zr 3d and O 1s is a removal of surface/interface oxygen species from the ZrO_2 particle/island surface. For the dry reforming reaction the peak shift - and the intensity change of the "dynamic" high BE O1s

compound (green) - is not as pronounced as for pure CH_4 because a 1:1 mixture of CH_4 and CO_2 was used. The gas atmosphere has therefore less reducing potential due to oxygen supply by CO_2. Prior and during exposure to CH_4 + CO_2 mixture, no carbon signal was observed in the C 1s spectra, and the Pt 4f signal remained at 71 eV. When increasing the reaction temperature to 773 and 873 K no further changes appeared in the Zr 3d, C 1s and Pt 4f spectra. Only the high binding energy component of the O 1s signal slightly shifted by 0.1 eV to 530.6 eV. These observations indicate that the ZrO_2 particles were stable during reaction up to 873 K. There was no formation of a ZrO_2 ultrathin film wetting the Pt surface and thus changing the amount of (reactive) sites. This shows that, at least under the applied conditions, no strong metal-support interaction (in the form of oxide wetting) occurred. Also, the surface stayed free of carbon deposits that would reduce the catalytic performance (a well-know effect especially for Ni catalysts). Only at lower reaction temperature (below ~500 K) carbon formation was observed. When the reaction temperature was raised from 773 to 873 K, mass spectroscopy detected minimal levels of CO/H_2 (not shown) but the active surface area of the inverse model catalyst (~1 cm^2) was too small for meaningful acquisition of catalytic data in the Bessy Setup.

4. Discussion

The current UHV and *in situ* XPS studies of an inverse model catalyst of ZrO_2 nanoislands on Pt(111) have shown that reducing conditions (UHV or CH_4) lead to the formation of an ultrathin ZrO_2 trilayer film partially covering the active Pt(111) surface. A schematics of the observed processes is presented in figure 6.

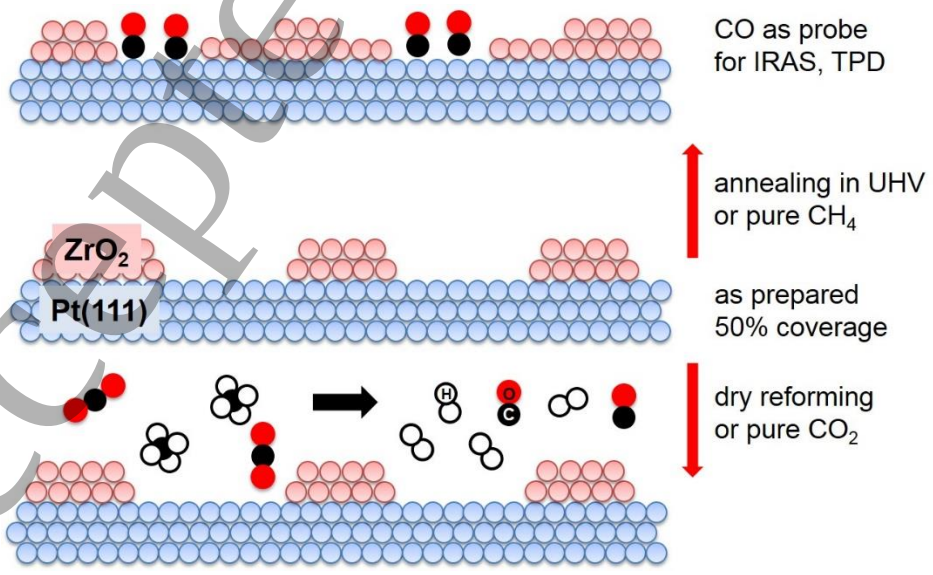

Figure 6: Scheme illustrating the ZrO_2/Pt(111) inverse model catalyst surface during the different experiments.

This relates our study to technological applications as strong metal-support interactions (SMSI) upon reduction in hydrogen can lead to an increase or loss of catalytic activity, depending on reduction temperature [45, 46, 77]. A possible explanation is that at increasing reduction temperatures the noble metals are successively covered due to the overgrowth of thin oxide layers (often considered as sub-oxides originating from the support) [78-81]. In the initial stages, this may create additional active metal-oxide interfaces but with successive encapsulation the metal may be fully blocked [82, 83]. Along these lines, Stagg-Williams et al. demonstrated that Pt/ZrO_2 catalysts reduced at 473 K showed higher activity for methane dry reforming than the catalyst reduced at 773 K [84]. Similarly, Faroldi et al. highlighted for dry reforming on Ru/La_2O_3–SiO_2 that reduction at 673 K induced higher activity than reduction at 823 K of the same catalyst [85]. Thus, for activation of noble metal catalysts, oxidation is typically followed rather by low temperature reduction.

Interestingly, also in the case of our inverse model catalyst, reducing conditions (UHV or CH_4) initiated SMSI, whereas (pure) CO_2 and the reaction environment (CO_2/CH_4 1:1 mixture) rather had a stabilizing effect on the ZrO_2 particle structure (and surface/interface oxygen), preventing the formation of a wetting ultrathin ZrO_2 film, thus preserving the active Pt surface area. Furthermore, during methane dry reforming at 673 – 873 K the surface remained free of any carbon deposits due to efficient carbon removal by CO_2 via the Boudouard reaction.

5. Conclusions

An inverse model catalyst of ZrO_2 clusters/islands supported on Pt(111) has been characterized after oxidation, when exposed to the individual reactants (CH_4 or CO_2) and *in situ* during the methane dry reforming reaction up to 873 K. The XPS data indicated that the ZrO_2 particles were reversibly wetting the Pt surface upon annealing (reduction) in UHV or under reducing (CH_4) conditions, via the formation of an ultrathin ZrO_2 trilayer film. Upon reoxidation in O_2 the initial ZrO_2 particle structure and surface/interface oxygen were reestablished. Infrared spectroscopy of the probe molecule CO adsorbed on Pt(111) was used for confirmation, as the on-top CO signal reversibly diminished and reappeared upon UHV annealing and reoxidation, respectively.

Exposure to pure CH_4 at reaction temperatures led to the formation of carbon deposits. By switching to pure CO_2 the surface carbon was easily removed via the Boudouard reaction. For the actual methane dry reforming reaction (CH_4/CO_2 1:1) the ZrO_2/Pt(111) inverse model catalyst was stable from 673 to 873 K. The Pt surface remained free of carbon and ZrO_2 remained in its oxidized state and island structure. In comparison to reducing UHV and pure CH_4 atmosphere, for which the formation of a wetting ZrO_2 trilayer film was observed, the dry reforming reaction environment was stabilizing the catalyst surface structure, preventing any SMSI effect to occur.

6. Acknowledgement

This work was supported by the Austrian Science Fund (FWF) through SFB "FOXSI" F4502, Project DryRef (I 942-N17), and DK "Solids4Fun" W1243, and through the European Community's Seventh Framework Programme (FP7/2007-2013) under grant agreement n.°312284. The authors gratefully acknowledge HZB/BESSY II for providing beamtime at the ISISS beamline and BESSY staff for continuous support during beamtime. We also want to thank MAX IV Laboratory for providing beamtime at the SPECIES beamline and its staff for continuous support.

Literature

[1] D. Pakhare, J. Spivey, A review of dry (CO2) reforming of methane over noble metal catalysts, Chemical Society Reviews, 43 (2014) 7813-7837.
[2] M.E.D. De Oliveira, B.E. Vaughan, E.J. Rykiel, Ethanol as fuels: Energy, carbon dioxide balances, and ecological footprint, Bioscience, 55 (2005) 593-602.
[3] M. Usman, W. Daud, H.F. Abbas, Dry reforming of methane: Influence of process parameters-A review, Renewable & Sustainable Energy Reviews, 45 (2015) 710-744.
[4] R. Schlogl, Sustainable Energy Systems: The Strategic Role of Chemical Energy Conversion, Topics in Catalysis, 59 (2016) 772-786.
[5] J.H. Lunsford, Catalytic conversion of methane to more useful chemicals and fuels: a challenge for the 21st century, Catalysis Today, 63 (2000) 165-174.
[6] J.R. Rostrupnielsen, PRODUCTION OF SYNTHESIS GAS, Catalysis Today, 18 (1993) 305-324.
[7] M.A. Pena, J.P. Gomez, J.L.G. Fierro, New catalytic routes for syngas and hydrogen production, Applied Catalysis a-General, 144 (1996) 7-57.
[8] D.J. Wilhelm, D.R. Simbeck, A.D. Karp, R.L. Dickenson, Syngas production for gas-to-liquids applications: technologies, issues and outlook, Fuel Processing Technology, 71 (2001) 139-148.
[9] P. Gangadharan, K.C. Kanchi, H.H. Lou, Evaluation of the economic and environmental impact of combining dry reforming with steam reforming of methane, Chemical Engineering Research & Design, 90 (2012) 1956-1968.

[10] G.A. Olah, A. Goeppert, M. Czaun, G.K.S. Prakash, Bi-reforming of Methane from Any Source with Steam and Carbon Dioxide Exclusively to Metgas (CO-2H(2)) for Methanol and Hydrocarbon Synthesis, Journal of the American Chemical Society, 135 (2013) 648-650.
[11] A.S. Larimi, S.M. Alavi, Ceria-Zirconia supported Ni catalysts for partial oxidation of methane to synthesis gas, Fuel, 102 (2012) 366-371.
[12] E. Ruckenstein, Y.H. Hul, Methane partial oxidation over NiO MgO solid solution catalysts, Applied Catalysis a-General, 183 (1999) 85-92.
[13] A.F. Lucredio, J.M. Assaf, E.M. Assaf, Reforming of a model biogas on Ni and Rh-Ni catalysts: Effect of adding La, Fuel Processing Technology, 102 (2012) 124-131.
[14] M.P. Kohn, M.J. Castaldi, R.J. Farrauto, Biogas reforming for syngas production: The effect of methyl chloride, Applied Catalysis B-Environmental, 144 (2014) 353-361.
[15] U. Izquierdo, V.L. Barrio, J. Requies, J.F. Cambra, M.B. Guemez, P.L. Arias, Tri-reforming: A new biogas process for synthesis gas and hydrogen production, International Journal of Hydrogen Energy, 38 (2013) 7623-7631.
[16] M.C.J. Bradford, M.A. Vannice, CO2 reforming of CH4, Catalysis Reviews-Science and Engineering, 41 (1999) 1-42.
[17] T. Wurzel, S. Malcus, L. Mleczko, Reaction engineering investigations of CO2 reforming in a fluidized-bed reactor, Chemical Engineering Science, 55 (2000) 3955-3966.
[18] T.A. Chubb, CHARACTERISTICS OF CO2-CH4 REFORMING-METHANATION CYCLE RELEVANT TO THE SOLCHEM THERMOCHEMICAL POWER SYSTEM, Solar Energy, 24 (1980) 341-345.
[19] D. Fraenkel, R. Levitan, M. Levy, A SOLAR THERMOCHEMICAL PIPE BASED ON THE CO2-CH4 (1-1) SYSTEM, International Journal of Hydrogen Energy, 11 (1986) 267-277.
[20] J.R.H. Ross, Natural gas reforming and CO2 mitigation, Catalysis Today, 100 (2005) 151-158.
[21] Y.H. Cui, H.D. Zhang, H.Y. Xu, W.Z. Li, Kinetic study of the catalytic reforming of CH4 with CO2 to syngas over Ni/alpha-Al2O3 catalyst: The effect of temperature on the reforming mechanism, Applied Catalysis a-General, 318 (2007) 79-88.
[22] C.E. Daza, J. Gallego, J.A. Moreno, F. Mondragon, S. Moreno, R. Molina, CO2 reforming of methane over Ni/Mg/Al/Ce mixed oxides, Catalysis Today, 133 (2008) 357-366.
[23] M.I. Dimitrijewits, M.M. Guraya, C.P. Arciprete, A.C. Luna, A. Becerra, Catalytic behaviour Ni/(y)-Al2O3 microporous catalysts in the methane dry-reforming reaction, Granular Matter, 3 (2001) 101-104.
[24] C.A.M. Abreu, D.A. Santos, J.A. Pacifico, N.M. Lima, Kinetic evaluation of methane-carbon dioxide reforming process based on the reaction steps, Industrial & Engineering Chemistry Research, 47 (2008) 4617-4622.
[25] K. Anic, A. Wolfbeisser, H. Li, C. Rameshan, K. Fottinger, J. Bernardi, G. Rupprechter, Surface Spectroscopy on UHV-Grown and Technological Ni-ZrO2 Reforming Catalysts: From UHV to Operando Conditions, Topics in Catalysis, 59 (2016) 1614-1627.
[26] Y.J.O. Asencios, E.M. Assaf, Combination of dry reforming and partial oxidation of methane on NiO-MgO-ZrO2 catalyst: Effect of nickel content, Fuel Processing Technology, 106 (2013) 247-252.
[27] A. Wolfbeisser, O. Sophiphun, J. Bernardi, J. Wittayakun, K. Fottinger, G. Rupprechter, Methane dry reforming over ceria-zirconia supported Ni catalysts, Catalysis Today, 277 (2016) 234-245.
[28] M.C.J. Bradford, M.A. Vannice, CO2 reforming of CH4 over supported Ru catalysts, Journal of Catalysis, 183 (1999) 69-75.
[29] M.F. Mark, W.F. Maier, CO2-reforming of methane on supported Rh and Ir catalysts, Journal of Catalysis, 164 (1996) 122-130.
[30] J.F. Munera, S. Irusta, L.M. Cornaglia, E.A. Lombardo, D.V. Cesar, M. Schmal, Kinetics and reaction pathway of the CO2 reforming of methane on Rh supported on lanthanum-based solid, Journal of Catalysis, 245 (2007) 25-34.
[31] A.M. O'Connor, Y. Schuurman, J.R.H. Ross, C. Mirodatos, Transient studies of carbon dioxide reforming of methane over Pt/ZrO2 and Pt/Al2O3, Catalysis Today, 115 (2006) 191-198.

[32] K. Nagaoka, K. Seshan, J.A. Lercher, K. Aika, Activation mechanism of methane-derived coke (CHx) by CO2 during dry reforming of methane - comparison for Pt/Al2O3 and Pt/ZrO2, Catalysis Letters, 70 (2000) 109-116.
[33] O. Demoulin, G. Rupprechter, I. Seunier, B. Le Clef, M. Navez, P. Ruiz, Investigation of parameters influencing the activation of a Pd/gamma-alumina catalyst during methane combustion, Journal of Physical Chemistry B, 109 (2005) 20454-20462.
[34] K.Y. Kung, P. Chen, F. Wei, G. Rupprechter, Y.R. Shen, G.A. Somorjai, Ultrahigh vacuum high-pressure reaction system for 2-infrared 1-visible sum frequency generation studies, Review of Scientific Instruments, 72 (2001) 1806-1809.
[35] M. Nemeth, Z. Schay, D. Sranko, J. Karolyi, G. Safran, I. Sajo, A. Horvath, Impregnated Ni/ZrO2 and Pt/ZrO2 catalysts in dry reforming of methane: Activity tests in excess methane and mechanistic studies with labeled (CO2)-C-13, Applied Catalysis a-General, 504 (2015) 608-620.
[36] M. Ocsachoque, F. Pompeo, G. Gonzalez, Rh-Ni/CeO2-Al2O3 catalysts for methane dry reforming, Catalysis Today, 172 (2011) 226-231.
[37] A. Wolfbeisser, G. Kovacs, S.M. Kozlov, K. Fottinger, J. Bernardi, B. Klotzer, K.M. Neyman, G. Rupprechter, Surface composition changes of CuNi-ZrO2 during methane decomposition: An operando NAP-XPS and density functional study, Catalysis Today, 283 (2017) 134-143.
[38] A. Wolfbeisser, B. Kloetzer, L. Mayr, R. Rameshan, D. Zemlyanov, J. Bernardi, K. Foettinger, G. Rupprechter, Surface modification processes during methane decomposition on Cu-promoted Ni-ZrO2 catalysts, Catalysis Science & Technology, 5 (2015) 967-978.
[39] K. Fottinger, G. Rupprechter, In Situ Spectroscopy of Complex Surface Reactions on Supported Pd-Zn, Pd-Ga, and Pd(Pt)-Cu Nanoparticles, Accounts of Chemical Research, 47 (2014) 3071-3079.
[40] T. Fuhrmann, M. Kinne, C.M. Whelan, J.F. Zhu, R. Denecke, H.P. Steinruck, Vibrationally resolved in situ XPS study of activated adsorption of methane on Pt(111), Chemical Physics Letters, 390 (2004) 208-213.
[41] J.H. Bitter, K. Seshan, J.A. Lercher, Mono and bifunctional pathways of CO2/CH4 reforming over Pt and Rh based catalysts, Journal of Catalysis, 176 (1998) 93-101.
[42] P. Ferreira-Aparicio, I. Rodriguez-Ramos, J.A. Anderson, A. Guerrero-Ruiz, Mechanistic aspects of the dry reforming of methane over ruthenium catalysts, Applied Catalysis a-General, 202 (2000) 183-196.
[43] J.M. Wei, E. Iglesia, Isotopic and kinetic assessment of the mechanism of reactions of CH4 with CO2 or H2O to form synthesis gas and carbon on nickel catalysts, Journal of Catalysis, 224 (2004) 370-383.
[44] M.C.J. Bradford, M.A. Vannice, Catalytic reforming of methane with carbon dioxide over nickel catalysts .1. Catalyst characterization and activity, Applied Catalysis a-General, 142 (1996) 73-96.
[45] D. Wang, S. Penner, D.S. Su, G. Rupprechter, K. Hayek, R. Schlogl, Silicide formation on a Pt /SiO2 model catalyst studied by TEM, EELS, and EDXS, Journal of Catalysis, 219 (2003) 434-441.
[46] S. Penner, D. Wang, D.S. Su, G. Rupprechter, R. Podloucky, R. Schlogl, K. Hayek, Platinum nanocrystals supported by silica, alumina and ceria: metal-support interaction due to high-temperature reduction in hydrogen, Surface Science, 532 (2003) 276-280.
[47] K. Hayek, M. Fuchs, B. Klotzer, W. Reichl, G. Rupprechter, Studies of metal-support interactions with "real" and "inverted" model systems: reactions of CO and small hydrocarbons with hydrogen on noble metals in contact with oxides, Topics in Catalysis, 13 (2000) 55-66.
[48] G. Rupprechter, A surface science approach to ambient pressure catalytic reactions, Catalysis Today, 126 (2007) 3-17.
[49] G. Rupprechter, Sum Frequency Generation and Polarization-Modulation Infrared Reflection Absorption Spectroscopy of Functioning Model Catalysts from Ultrahigh Vacuum to Ambient Pressure, Advances in Catalysis, Vol 51, 51 (2007) 133-263.
[50] G. Rupprechter, Surface vibrational spectroscopy from ultrahigh vacuum to atmospheric pressure: adsorption and reactions on single crystals and nanoparticle model catalysts monitored by sum frequency generation spectroscopy, Physical Chemistry Chemical Physics, 3 (2001) 4621-4632.

[51] G. Rupprechter, T. Dellwig, H. Unterhalt, H.J. Freund, High-pressure carbon monoxide adsorption on Pt(111) revisited: A sum frequency generation study, Journal of Physical Chemistry B, 105 (2001) 3797-3802.
[52] L. Mayr, N. Koepfle, A. Auer, B. Kloetzer, S. Penner, An (ultra) high-vacuum compatible sputter source for oxide thin film growth, Review of Scientific Instruments, 84 (2013).
[53] H. Li, J.-I.J. Choi, W. Mayr-Schmoelzer, C. Weilach, C. Rameshan, F. Mittendorfer, J. Redinger, M. Schmid, G. Rupprechter, Growth of an Ultrathin Zirconia Film on Pt3Zr Examined by High-Resolution X-ray Photoelectron Spectroscopy, Temperature-Programmed Desorption, Scanning Tunneling Microscopy, and Density Functional Theory, Journal of Physical Chemistry C, 119 (2015) 2462-2470.
[54] P. Lackner, J.I.J. Choi, U. Diebold, M. Schmid, Construction and evaluation of an ultrahigh-vacuum-compatible sputter deposition source, Review of Scientific Instruments, 88 (2017).
[55] P. Hollins, Infrared Reflection–Absorption Spectroscopy, In Encyclopedia of Analytical Chemistry, John Wiley & Sons, 2000.
[56] H. Michael, Innovative Station for In Situ Spectroscopy . in, 2016.
[57] J. Schnadt, J. Knudsen, J.N. Andersen, H. Siegbahn, A. Pietzsch, F. Hennies, N. Johansson, N. Martensson, G. Ohrwall, S. Bahr, S. Mahl, O. Schaff, The new ambient-pressure X-ray photoelectron spectroscopy instrument at MAX-lab, Journal of Synchrotron Radiation, 19 (2012) 701-704.
[58] S. Urpelainen, C. Sathe, W. Grizolli, M. Agaker, A.R. Head, M. Andersson, S.W. Huang, B.N. Jensen, E. Wallen, H. Tarawneh, R. Sankari, R. Nyholm, M. Lindberg, P. Sjoblom, N. Johansson, B.N. Reinecke, M.A. Arman, L.R. Merte, J. Knudsen, J. Schnadt, J.N. Andersen, F. Hennies, The SPECIES beamline at the MAX IV Laboratory: a facility for soft X-ray RIXS and APXPS, Journal of Synchrotron Radiation, 24 (2017) 344-353.
[59] NIST Electron Effective-Attenuation-Length Database, in, The National Institute of Standards and Technology (NIST), http://www.nist.gov/srd/nist82.cfm.
[60] C. Rameshan, M.L. Ng, A. Shavorskiy, J.T. Newberg, H. Bluhm, Water adsorption on polycrystalline vanadium from ultra-high vacuum to ambient relative humidity, Surface Science, 641 (2015) 141-147.
[61] Y. Gao, L. Zhang, Y. Pan, G. Wang, Y. Xu, W. Zhang, J. Zhu, Epitaxial growth of ultrathin ZrO2(111) films on Pt(111), Chinese Science Bulletin, 56 (2011) 502-507.
[62] J.I.J. Choi, W. Mayr-Schmoelzer, F. Mittendorfer, J. Redinger, U. Diebold, M. Schmid, The growth of ultra-thin zirconia films on Pd3Zr(0001), Journal of Physics-Condensed Matter, 26 (2014).
[63] M. Antlanger, W. Mayr-Schmolzer, J. Pavelec, F. Mittendorfer, J. Redinger, P. Varga, U. Diebold, M. Schmid, Pt3Zr(0001): A substrate for growing well-ordered ultrathin zirconia films by oxidation, Physical Review B, 86 (2012).
[64] B.E. Hayden, A.M. Bradshaw, THE ADSORPTION OF CO ON PT(111) STUDIED BY INFRARED REFLECTION-ABSORPTION SPECTROSCOPY, Surface Science, 125 (1983) 787-802.
[65] G. Rupprechter, T. Dellwig, H. Unterhalt, H.J. Freund, CO adsorption on Ni(100) and Pt(111) studied by infrared-visible sum frequency generation spectroscopy: design and application of an SFG-compatible UHV-high-pressure reaction cell, Topics in Catalysis, 15 (2001) 19-26.
[66] D.E. Starr, E.K. Wong, D.R. Worsnop, K.R. Wilson, H. Bluhm, A combined droplet train and ambient pressure photoemission spectrometer for the investigation of liquid/vapor interfaces, Physical Chemistry Chemical Physics, 10 (2008) 3093-3098.
[67] G. Binnig, C.F. Quate, C. Gerber, ATOMIC FORCE MICROSCOPE, Physical Review Letters, 56 (1986) 930-933.
[68] C. Rameshan, W. Stadlmayr, C. Weilach, S. Penner, H. Lorenz, M. Havecker, R. Blume, T. Rocha, D. Teschner, A. Knop-Gericke, R. Schlogl, N. Memmel, D. Zemlyanov, G. Rupprechter, B. Klotzer, Subsurface-Controlled CO2 Selectivity of PdZn Near-Surface Alloys in H-2 Generation by Methanol Steam Reforming, Angewandte Chemie-International Edition, 49 (2010) 3224-3227.
[69] D.J. Miller, H. Oberg, S. Kaya, H.S. Casalongue, D. Friebel, T. Anniyev, H. Ogasawara, H. Bluhm, L.G.M. Pettersson, A. Nilsson, Oxidation of Pt(111) under Near-Ambient Conditions, Physical Review Letters, 107 (2011).

[70] V.I. Bukhtiyarov, V.V. Kaichev, The combined application of XPS and TPD to study of oxygen adsorption on graphite-supported silver clusters, Journal of Molecular Catalysis a-Chemical, 158 (2000) 167-172.
[71] Y. Do, J.S. Choi, S.K. Kim, Y. Sohn, The Interfacial Nature of TiO2 and ZnO Nanoparticles Modified by Gold Nanoparticles, Bulletin of the Korean Chemical Society, 31 (2010) 2170-2174.
[72] P.R. Norton, J.W. Goodale, E.B. Selkirk, ADSORPTION OF CO ON PT(111) STUDIED BY PHOTOEMISSION, THERMAL-DESORPTION SPECTROSCOPY AND HIGH-RESOLUTION DYNAMIC MEASUREMENTS OF WORK FUNCTION, Surface Science, 83 (1979) 189-227.
[73] M.A. Petersen, S.J. Jenkins, D.A. King, Theory of methane dehydrogenation on Pt{110}(1x2). Part 1: Chemisorption of CHx (x=0-3), Journal of Physical Chemistry B, 108 (2004) 5909-5919.
[74] T. Fuhrmann, M. Kinne, B. Trankenschuh, C. Papp, J.F. Zhu, R. Denecke, H.P. Steinruck, Activated adsorption of methane on Pt(111) - an in situ XPS study, New Journal of Physics, 7 (2005).
[75] M. Souza, M. Schmal, Methane conversion to synthesis gas by partial oxidation and CO2 reforming over supported platinum catalysts, Catalysis Letters, 91 (2003) 11-17.
[76] D. Qin, J. Lapszewicz, STUDY OF MIXED STEAM AND CO2 REFORMING OF CH4 TO SYNGAS ON MGO-SUPPORTED METALS, Catalysis Today, 21 (1994) 551-560.
[77] K. Hayek, H. Goller, S. Penner, G. Rupprechter, C. Zimmermann, Regular alumina-supported nanoparticles of iridium, rhodium and platinum under hydrogen reduction: structure, morphology and activity in the neopentane conversion, Catalysis Letters, 92 (2004) 1-9.
[78] G. Rupprechter, G. Seeber, H. Goller, K. Hayek, Structure-activity correlations on Rh/Al2O3 and Rh/TiO2 thin film model catalysts after oxidation and reduction, Journal of Catalysis, 186 (1999) 201-213.
[79] S.J. Tauster, S.C. Fung, STRONG METAL-SUPPORT INTERACTIONS - OCCURRENCE AMONG BINARY OXIDES OF GROUPS IIA-VB, Journal of Catalysis, 55 (1978) 29-35.
[80] W. Unterberger, B. Jenewein, B. Klotzer, S. Penner, W. Reichl, G. Rupprechter, D. Wang, R. Schlogl, K. Hayek, Hydrogen-induced metal-oxide interaction studied on noble metal model catalysts, Reaction Kinetics and Catalysis Letters, 87 (2006) 215-234.
[81] M. Fuchs, B. Jenewein, S. Penner, K. Hayek, G. Rupprechter, D. Wang, R. Schlogl, J.J. Calvino, S. Bernal, Interaction of Pt and Rh nanoparticles with ceria supports: Ring opening of methylcyclobutane and CO hydrogenation after reduction at 373-723 K, Applied Catalysis a-General, 294 (2005) 279-289.
[82] F. Pesty, H.P. Steinruck, T.E. Madey, THERMAL-STABILITY OF PT FILMS ON TIO2(110) - EVIDENCE FOR ENCAPSULATION, Surface Science, 339 (1995) 83-95.
[83] O. Dulub, W. Hebenstreit, U. Diebold, Imaging cluster surfaces with atomic resolution: The strong metal-support interaction state of Pt supported on TiO2(110), Physical Review Letters, 84 (2000) 3646-3649.
[84] S.M. Stagg-Williams, F.B. Noronha, G. Fendley, D.E. Resasco, CO2 reforming of CH4 over Pt/ZrO2 catalysts promoted with La and Ce oxides, Journal of Catalysis, 194 (2000) 240-249.
[85] B.M. Faroldi, E.A. Lombardo, L.M. Cornaglia, Surface properties and catalytic behavior of Ru supported on composite La2O3-SiO2 oxides, Applied Catalysis a-General, 369 (2009) 15-26.